Metal–organic frameworks for the capture of α-pinene traces

Patrick Conti, Kamal Batra, Paul Iacomi, Carla Vieira Soares, Sanchari Dasgupta, Nathalie Steunou, Agnès Lattuati-Derieux, Noëlle Timbart, Mélanie Nicolas, Rukshala Anton, et al.

ChemComm

Metal–organic frameworks for the capture of α-pinene traces†

Patrick P. Conti,‡[ab] Kamal Batra,‡[a] Paul Iacomi,[a] Carla Vieira Soares,[a] Sanchari Dasgupta, [c] Nathalie Steunou, [c] Agnès Lattuati-Derieux,[d] Noëlle Timbart,[d] Mélanie Nicolas,[b] Rukshala Anton,[b] Stéphane Moularat,[b] Guillaume Maurin [a] and Sabine Devautour-Vinot [a]*

A dual computational/experimental approach enabled ranking of the performance of a series of MOFs for α-pinene capture in terms of affinity and uptake. UiO-66(Zr) is demonstrated to be a good candidate for adsorbing α-pinene at sub-ppm levels, while MIL-125(Ti)-NH₂ shows ideal performances for abating α-pinene at concentrations encountered in indoor air.

Terpenes are Volatile Organic Compounds (VOCs) of biogenic or anthropological sources, emitted in indoor environments from plants, wooden building materials, organic solvents or household, cosmetic, fragranced, and cooking products.[1–4] Indoor terpene concentration substantially varies depending on the occupant activities: it usually ranges from 0.01 to 270.00 μg m⁻³ and can reach up to 6000 μg m⁻³ after using cleaning products.[1,5–7] The impact of terpenes on human health is limited to irritating and/or allergenic effects.[3] However, their isoprene structure makes them very reactive with ozone, hydroxyl, or nitrate radicals even at low concentration, resulting in oxidation by-products, *e.g.* gas species, formaldehyde, acetic acid, and ultrafine particles, which are much more harmful than the terpene precursors themselves.[8,9] Therefore, the development of solutions to mitigate indoor air contamination by terpenes is of utmost importance. Noteworthy, this problematic is also relevant in cultural heritage institutions,[10,11]

not only to protect visitors and employers but also to preserve art collections from damage.[12–14] In this context, terpene contamination in enclosed spaces such as display cases, archive boxes, archive magazines, or storage rooms can exceed that of the surrounding indoor air. The pollution sources comprise the materials constituting these spaces, the essential oils used in the process of Egyptian mummification, the biocides treatments, solvents of products of restorations, among others combined with a weak air renewal of the atmosphere supporting the concentration of the compounds around the heritage works.

Post-processing technologies have been developed for the removal of a wide range of VOCs from indoor air. They are based on destructive methods, *i.e.* catalytic and thermal oxidation, biodegradation and plasma catalysis, or recovery approaches, *i.e.* membrane separation, absorption, condensation, and adsorption.[15,16] Adsorption-based process using sorbent materials, is regarded as the most efficient technology for VOCs abatement from air, since it combines simple operating technology, low maintenance cost, and low energy consumption with the ability to recover and reuse both sorbent materials and VOCs.[15,17,18] A large panel of porous solids has been explored for VOCs capture,[17,18] including mesoporous silica,[19] zeolites,[20] carbonaceous materials,[21] and Metal–organic frameworks (MOFs).[22] MOFs are one of the most recent classes of porous solids, constructed through an almost infinite combination of metal ions and organic polydentate ligands. They have been identified as promising candidates over the traditional porous materials for the sorption of a wide range of indoor and outdoor contaminants (CO_x, NO_x, SO_x)[23,24] as well as diverse VOCs (aldehydes, ketones, acids, alcohols, and aromatics).[25–28] Their attractiveness for VOCs capture, even at trace levels, relies on their unique richness in terms of structural and chemical features that can be modulated to favour a strong affinity for the target VOC *via* electrostatic interactions, π-complex formation, hydrogen bonding or even throughout geometric confinement.[25–27] In addition, MOF materials containing high-valence metal ions have been demonstrated to be highly

a Institut Charles Gerhardt Montpellier (ICGM), UMR 5253 – CNRS/UM/ENSCM, Pole Chimie Balard Recherche, Montpellier cedex 5 34293, France. E-mail: sabine.devautour-vinot@umontpellier.fr

b Centre Scientifique et Technique du Bâtiment (CSTB), 24 rue Joseph Fournier, Saint-Martin-d'Hères 38400, France

c Institut Lavoisier de Versailles (ILV), UMR 8180, Université de Versailles St Quentin en Yvelines, Université Paris Saclay, Versailles cedex 78035, France

d Centre de Recherche et de Restauration des Musées de France (C2RMF), Département Recherche, Palais du Louvre, 14 quai François Mitterrand, Paris 75001, France

† Electronic supplementary information (ESI) available: Sample synthesis and characterization, calibration procedure of DVS inlet mixture, computational details, MC configurations for α-pinene in UiO-66(Zr) and DUT-4(Al) are supplied as Supporting Information. See DOI: https://doi.org/10.1039/d3cc01724a

‡ These authors contributed equally to this work.

chemically stable which is of crucial interest for their long-term use under working conditions.[29] So far, only a very few porous coordination polymers (MOFs and COFs, *i.e.* covalent organic frameworks) have been explored for their sorption-related properties towards terpenes, mostly for terpenes enantioselective separation in liquid phase and sensing applications.[30–33] Although this family of porous materials has shown promises for the adsorption of terpenes at high VOC concentrations, their performance for the challenging capture of airborne terpenes traces has never been addressed until now.

Herein, a series of microporous MOFs was explored using a dual experimental/modelling approach to identify sorbents which combine high terpene affinity and substantial sorption terpene uptake at low terpene airborne concentration. α-pinene, *i.e.* $C_{10}H_{16}$, was considered as a representative molecule of this family of airborne contaminant, since it is the most commonly terpene species encountered in indoor environments.[34] We selected well-known MOFs with pore sizes compatible with hosting α-pinene (kinetic diameter $\varnothing_{\alpha\text{-pinene}}$ = 7 Å) while showing an easy synthesis route and high chemical/thermal stability. Accordingly, the microporous MOFs, UiO-66(Zr), MIL-125(Ti)-NH$_2$, Cr-soc-mof, MIL-68(Al), DUT-4(Al), and DUT-5(Al), with distinct pore structures (cage- and tunnel-like porosity), chemical features (ligand nature/functionalisation) and pore dimension/volume, were examined for the capture of α-pinene traces. Periodic Density Functional Theory (DFT) and Force Field Monte Carlo (MC) simulations were first carried out to assess the α-pinene affinity of these MOFs with the objective to select the most promising ones for further experimental testing. Therefore, UiO-66(Zr), MIL-125(Ti)-NH$_2$, and DUT-4(Al) were subsequently investigated by recording their α-pinene gravimetric sorption isotherms at 303 K in the [0.2 - 1000] ppm concentration range. UiO-66(Zr) was demonstrated to be the best candidate for α-pinene capture at traces level, *i.e.* $C_{\alpha\text{-pinene}}$ < 0.2 ppm (<1.1 mg m^{-3}), while MIL-125(Ti)-NH$_2$ was found to be efficient for adsorbing α-pinene at higher concentration, *i.e.* $C_{\alpha\text{-pinene}}$ > 0.8 ppm (>4.5 mg m^{-3}). MC simulations were further deployed to reveal the preferential location of α-pinene in these selected MOFs at various analyte loadings.

Periodic DFT calculations and MC simulations first revealed the preferential orientations of α-pinene within the pores of UiO-66(Zr), MIL-125(Ti)-NH$_2$, Cr-soc-mof, MIL-68(Al), DUT-4(Al), and DUT-5(Al) at low loading and assessed the resulting strength of guest-host framework interactions. The DFT-calculated α-pinene/MOF interaction energies (E_{int}) along with their MC simulated adsorption enthalpies (ΔH_{ads}) are reported in Table 1. Both simulated energetics correlate well and this validates the force field parameters/charges used to describe the host/guest interactions in the MC calculations. Notably, these simulations evidenced that UiO-66(Zr) shows the strongest interactions with α-pinene followed by MIL-125(Ti)-NH$_2$ while the other 4 MOFs show similar moderate interaction energies, in line with a lowering of the α-pinene confinement (larger pore size of these last 4 MOFs). The DFT-calculated α-pinene interaction energy (E_{int}) of -116.2 kJ mol^{-1}

Table 1 DFT-simulated pinene/MOF interaction energies (E_{int}) and MC-calculated pinene/MOF adsorption enthalpies at low coverage (ΔH_{ads})

MOF Structures	E_{int} kJ mol^{-1}	ΔH_{ads} kJ mol^{-1}
UiO-66(Zr)	−116.2	−99.7
MIL-125(Ti)-NH$_2$	−91.8	−76.2
Cr-soc-mof	−64.5	−75.2
MIL-68(Al)	−56.2	−48.0
DUT-4(Al)	−56.4	−60.0
DUT-5(Al)	−53.2	−55.6

for UiO-66(Zr) is associated to the preferential sitting of α-pinene in the tetrahedral cage of this MOF as illustrated in Fig. 1a. A consequence of this highly confined environment is to enable the interactions of α-pinene with both the μ–OH functions of the inorganic node and the organic linker of the MOF with associated short separating distances, *e.g.* dC(–CH$_3$, α-pinene)–H(μ$_3$OH, MOF) = 2.69 Å, and dC(–CH, α-Pinene)–C(terephthalate, MOF) = 2.82 Å (Fig. 1a). α-pinene was equally found to preferentially adsorb in the smaller cages of MIL-125(Ti)-NH$_2$ interacting with both the carboxylate group and the –NH$_2$ functional group of the organic linker with representative distances of dH(–CH$_2$, α-pinene)–O(COO-MOF) = 2.68 Å, ii). dH(–CH, α-pinene)–N(NH$_2$)-MOF = 2.69 Å (Fig. 1b). The weaker interactions between α-pinene and the other 4 MOFs are associated to the low degree of pore confinement. Typically Fig. 1c reports the preferential geometry of α-pinene adopted in the channel of DUT-4(Al) revealing that the guest molecule interacts mostly with the organic linker with the shortest separating distance of about 3Å.

Besides the host/guest affinity at low concentration, the sorption capacity is an additional key metric for assessing the ability of porous sorbents to capture traces of contaminants in air. The sorption isotherm of α-pinene was then collected for the two MOFs predicted with the strongest interactions with this analyte, *i.e.* UiO-66(Zr) and MIL-125(Ti)-NH$_2$, as well as one representative MOF with a moderate affinity, *i.e.* DUT-4(Al). These MOF samples were prepared according to the procedures detailed in the SI. The characterization of these MOFs by combining PXRD, FT-IR, TGA, and N$_2$ physisorption firstly confirmed that these MOFs were successfully synthesized as pure phases (*cf.* Fig. S1, S2, S4–S6, ESI†). Their textural properties such as theoretical N$_2$-accessible surface area and free pore volume along with the experimental S_{BET} and V_{pore} are reported in Table S1 (ESI†). The α-pinene sorption isotherms were further collected using a gravimetric system *in-house* modified to create very low partial pressures of α-pinene by diluting the analyte vapour in an inert carrier gas. Minute concentrations of α-pinene down to 0.2 ppm (= 1.1 mg m^{-3}) could be achieved, in line with the terpene contamination conditions encountered in indoor air. Fig. 2 displays the α-pinene adsorption isotherms collected at 303 K, in the [0.2–1000] ppm concentration range. A type I profile with a step-wise increase of the α-pinene uptake was observed at low coverage, *i.e.* for the sorbate concentration lower than 300 ppm for the tested 3 MOFs.

At the highest concentration range, the adsorption uptake merges toward 0.38 g g^{-1}, 0.43 g g^{-1}, and 0.48 g g^{-1},
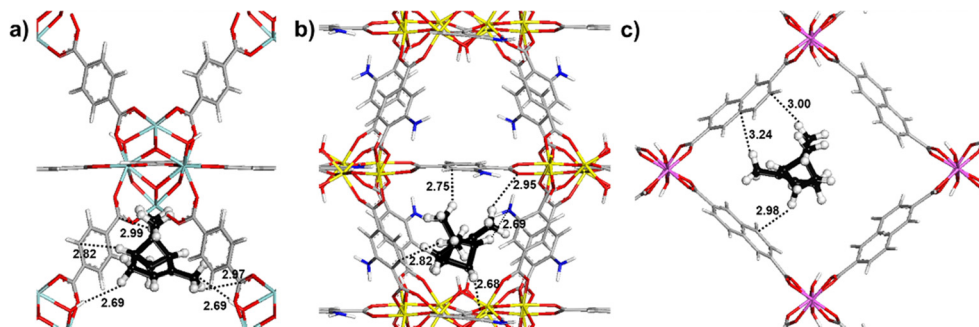
Fig. 1 DFT-simulated preferential sitting of α-pinene in (a) UiO-66(Zr), (b) MIL-125(Ti)-NH$_2$, and (c) DUT-4(Al). The characteristic guest/MOF interacting distances (dotted lines) are reported in Å. Color codes for the MOF framework atoms: hydrogen (white), carbon (light grey), nitrogen (blue), oxygen (red), zirconium (cyan), titanium (yellow), aluminum (pink), and for the α-pinene atoms: hydrogen (white) and carbon (black).
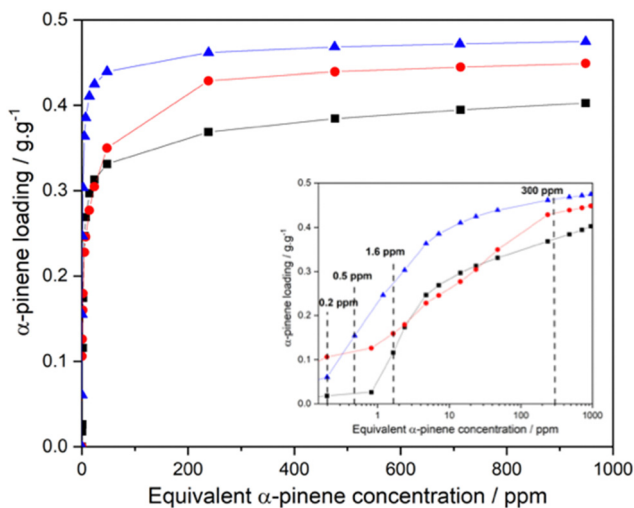

Fig. 2 α-pinene gravimetric sorption isotherm for UiO-66(Zr) (red circle), MIL-125(Ti)-NH$_2$ (blue triangle), and DUT-4(Al) (black square), collected in the equivalent 0–1000 ppm concentration range at 1 atm, 303 K. The insert shows the semi-logarithmic scale plot.

for DUT-4(Al), UiO-66(Zr), and MIL-125(Ti)-NH$_2$, respectively. More interestingly these three MOFs exhibit distinct sorption behaviours at low analyte concentration as magnified by the semi-logarithm plot of the adsorption isotherms shown in the inset of Fig. 2. The uptake of α-pinene for UiO-66(Zr) is almost linear with increasing the logarithm of the analyte concentration up to 300 ppm. The starting concentration point at 0.2 ppm results in a significant α-pinene uptake of 0.11 g g^{-1}. Noteworthy, we can extrapolate from our experimental collected data that UiO-66(Zr) is still able to adsorb α-pinene below 0.2 ppm although it cannot be fully confirmed by using our apparatus in this range of ultra-low concentration of the analyte. On the opposite, the two other MOFs show a sigmoidal sorption isotherm, with a negligible adsorbed amount of α-pinene at 0.2 ppm. Indeed, MIL-125(Ti)-NH$_2$ and DUT-4(Al) start to adsorb at about 0.8 ppm and 1.6 ppm respectively. This low concentration sorption sequence is in line with the simulated affinity order UiO-66(Zr) > MIL-125(Ti)-NH$_2$ > DUT-4(Al) (Table 1).

Therefore, UiO-66(Zr) combines the strongest affinity toward α-pinene with the highest capacity at 0.2 ppm, making it as the optimal solid for adsorbing α-pinene at sub-ppm levels. For capturing α-pinene at higher analyte concentration, i.e. from 1.6 to 10 ppm, the three selected MOFs efficiently adsorb the contaminant, while MIL-125(Ti)-NH$_2$ shows higher uptake compared to the two other structures. As a consequence, MIL-125(Ti)-NH$_2$ is the best candidate for abating α-pinene at concentrations found in indoor air condition ([270–6000] μg m^3, i.e. [0.05–1.08] ppm).

To gain insight into the α-pinene sorption mechanism in MIL-125(Ti)-NH$_2$ for the target range of analyte concentration (<20 ppm) we performed complementary MC simulations in the canonical ensemble for different loadings fixed from the experimental adsorption isotherms. At the very initial stage of adsorption, α-pinene is located in the smallest cage and interacts with both the μ–OH groups and the carbons of the organic linker (Fig. 3a and b) in line with the geometries obtained by DFT calculations (Fig. 1b). Fig. 3c depicts that at 1.0 ppm the cages are filled by a larger concentration of molecules establishing guest/guest interactions with associated intermolecular separating molecule-molecule distance of 2.1 Å. At higher concentration (14 ppm) the tetrahedral cages are fully occupied by the guest molecules and then the octahedral cages start to be filled, (Fig. 3d).

The α-pinene sorption mechanism was also investigated for the two other MOFs (Fig. S7, ESI†) in the target range of analyte concentration. Fig. S7b (ESI†) shows that the molecule preferentially adsorbs in the tetrahedral cage of UiO-66(Zr) at the very initial stage of adsorption. in line with the DFT predicted one (Fig. 1c). α-pinene then populates all tetrahedral cages in the range of concentration up to 24 ppm (Fig. S7d, ESI†) and the octahedral cages are only occupied at high concentrations (Fig. S7e, ESI†). Finally, DUT-4(Al) does not exhibit any strong anchoring site for α-pinene at low concentration (Fig. S8a, ESI†) interacting only via weak van der Waals interactions with the organic linker and filling the channel at 1.6 ppm (Fig. S8c, ESI†).

In conclusion, various microporous MOFs were explored for α-pinene capture at concentrations found in indoor air. Among
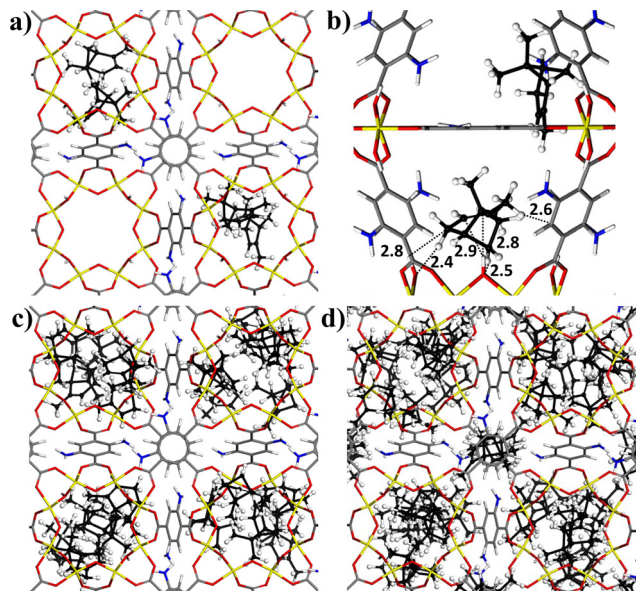
Fig. 3 Monte Carlo configurations for α-pinene in MIL-125(Ti)-NH$_2$ at different analyte loadings determined from the experimental adsorption isotherm at (a) and (b) low concentration (0.06 g g^{-1} = 0.44 mmol g^{-1} with host-guest interacting distances reported in Å, (c) 1.2 ppm (0.24 g g^{-1} = 1.81 mmol g^{-1}), and (d) 14 ppm (0.41 g g^{-1} = 3.0 mmol g^{-1}).

them, MIL-125(Ti)-NH$_2$ is demonstrated as a good competitor, as it displays both high uptake and optimal affinity toward α-pinene. Interestingly, the adsorption of α-pinene by MIL-125(Ti)-NH$_2$ is irreversible at 303 K (cf. Fig. S9, ESI†), while the solid is fully regenerated under mild conditions, i.e. at 373 K, under secondary vacuum.

Conflicts of interest

There are no conflicts to declare.

Notes and references

1 S. Angulo Milhem, M. Verriele, M. Nicolas and F. Thevenet, Environ. Sci. Pollut. Res., 2020, 27, 14365–14411.

2 C. M. Wang, B. Barratt, N. Carslaw, A. Doutsi, R. E. Dunmore, M. W. Ward and A. C. Lewis, Environ. Sci.: Processes Impacts, 2017, 19, 528–537.

3 D. A. Sarigiannis, S. P. Karakitsios, A. Gotti, I. L. Liakos and A. Katsoyiannis, Environ. Int., 2011, 34, 743–765.

4 S. Rovelli, A. Cattaneo, A. Fazio, A. Spinazzè, F. Borghi, D. Campagnolo, C. Dossi and D. M. Cavallo, Atmosphere, 2019, 10, 57.

5 B. C. Singer, H. Destaillats, A. T. Hodgson and W. W. Nazaroff, Indoor Air, 2006, 16, 179–191.

6 S. Angulo Milhem, M. Verriele, M. Nicolas and F. Thevenet, Atmos. Environ., 2021, 246, 118060.

7 S. Angulo-Milhem, M. Verriele, M. Nicolas and F. Thevenet, Atmos. Environ., 2021, 244, 117863.

8 P. Wolkoff, Int. J. Hyg. Environ. Health, 2020, 225, 113439.

9 A. C. Rohr, Environ. Int., 2013, 60, 145–162.

10 T. Martellini, C. Berlangieri, L. Dei, E. Carretti, S. Santini, A. Barone and A. Cincinelli, Indoor Air, 2020, 30, 900–913.

11 P. Clair, N. Leclerc, E. Rivière and G. Markut, ASPA, 2008, 1–18.

12 J. Tétreault, A. L. Dupont, P. Bégin and S. Paris, Polym. Degrad. Stab., 2013, 92, 1827–1837.

13 A. Alvarez-Martin, M. Wilcop, R. Anderson, D. Wendt, R. Barden and G. M. Kavich, Air Qual., Atmos. Health, 2021, 14, 1797–1809.

14 O. Chiantore and T. Poli, Atmosphere, 2021, 12, 364.

15 X. Li, L. Zhang, Z. Yang, P. Wang, Y. Yan and J. Ran, Sep. Purif. Technol., 2020, 235, 116213.

16 X. Yue, N. L. Ma, C. Sonne, R. Guan, S. S. Lam, Q. Van Le, X. Chen, Y. Yang, H. Gu, J. Rinklebe and W. Peng, J. Hazard. Mater., 2021, 405, 124138.

17 E. Hunter-Sellars, J. J. Tee, I. P. Parkin and D. R. Williams, Microporous Mesoporous Mater., 2020, 298, 110090.

18 L. Zhu, D. Shen and K. H. Luo, J. Hazard. Mater., 2020, 389, 122102.

19 M. F. Attia, M. I. Swasy, M. Ateia, F. Alexis and D. C. Whitehead, Chem. Commun., 2020, 56, 607–610.

20 K. M. Lee, N. S. Kim, M. Numan, J. C. Kim, H. S. Cho, K. Cho and C. Jo, ACS Appl. Mater. Interfaces, 2021, 13, 53925–53934.

21 K. Zhou, W. Ma, Z. Zeng, X. Ma, X. Xu, Y. Guo, H. Li and L. Li, Chem. Eng. J., 2019, 372, 1122–1133.

22 E. Barea, C. Montoro and J. A. R. Navarro, Chem. Soc. Rev., 2014, 43, 5419–5430.

23 E. Martínez-Ahumada, M. L. Díaz-Ramírez, M. de, J. Velásquez-Hernández, V. Jancik and I. A. Ibarra, Chem. Sci., 2021, 12, 6772–6799.

24 J. Bin Lin, T. T. T. Nguyen, R. Vaidhyanathan, J. Burner, J. M. Taylor, H. Durekova, F. Akhtar, R. K. Mah, O. Ghaffari-Nik, S. Marx, N. Fylstra, S. S. Iremonger, K. W. Dawson, P. Sarkar, P. Hovington, A. Rajendran, T. K. Woo and G. K. H. Shimizu, Science, 2021, 374, 1464–1469.

25 K. Dedecker, E. Dumas, B. Lavédrine, N. Steunou and C. Serre, Metal–Organic Frameworks (MOFs) for Environmental Applications, 2019, pp. 141–178.

26 P. Kumar, E. Vejerano, A. Khan, G. Lisak, J. H. Ahn and K. H. Kim, Korean J. Chem. Eng., 2019, 36, 1839–1853.

27 M. S. Yao, W. H. Li and G. Xu, Coord. Chem. Rev., 2021, 426, 213479.

28 M. I. Severino, A. Al Mohtar, C. Vieira Soares, C. Freitas, N. Sadovnik, S. Nandi, G. Mouchaham, V. Pimenta, F. Nouar, M. Daturi, G. Maurin, M. L. Pinto and C. Serre, Angew. Chem., 2023, 135, e202211583.

29 S. Yuan, L. Feng, K. Wang, J. Pang, M. Bosch, C. Lollar, Y. Sun, J. Qin, X. Yang, P. Zhang, Q. Wang, L. Zou, Y. Zhang, L. Zhang, Y. Fang, J. Li and H. C. Zhou, Adv. Mater., 2018, 30, 1704303.

30 Z. G. Gu, S. Grosjean, S. Bräse, C. Wöll and L. Heinke, Chem. Commun., 2015, 51, 8998–9001.

31 X. Hou, T. Xu, Y. Wang, S. Liu, J. Tong and B. Liu, ACS Appl. Mater. Interfaces, 2017, 9, 32264–32269.

32 X. Wu, X. Han, Q. Xu, Y. Liu, C. Yuan, S. Yang, Y. Liu, J. Jiang and Y. Cui, J. Am. Chem. Soc., 2019, 141, 7081–7089.

33 Y. Liu, L. Liu, X. Chen, Y. Liu, Y. Han and Y. Cui, J. Am. Chem. Soc., 2021, 143, 3509–3518.

34 Y. Noma and Y. Asakawa, Comprehensive Natural Products II: Chemistry and Biology, 2010, pp. 669–801.